© 2017. Published by The Company of Biologists Ltd | Development (2017) 144, 530 doi:10.1242/dev.148460

CORRECTION

Correction: Chondrocytic ephrin B2 promotes cartilage destruction by osteoclasts in endochondral ossification

Stephen Tonna, Ingrid J. Poulton, Farzin Taykar, Patricia W. M. Ho, Brett Tonkin, Blessing Crimeen-Irwin, Liliana Tatarczuch, Narelle E. McGregor, Eleanor J. Mackie, T. John Martin and Natalie A. Sims

There was an error published in Development **143**, 648-657.

In the Materials and Methods section the murine *Efnb2* gene mutation was incorrectly listed as $Efnb2^{tm1And}$. The correct annotation for the floxed allele that we used in our experiments is $Efnb2^{tm2And}$. This was a nomenclature error and does not affect the results or conclusions of the paper.

We thank Monika Tomczuk, scientific curator of Mouse Genome Informatics at The Jackson Laboratory, for alerting us to this mistake.

We apologise for any confusion that this error may have caused.

© 2016. Published by The Company of Biologists Ltd | Development (2016) 143, 648-657 doi:10.1242/dev.125625

RESEARCH ARTICLE

Chondrocytic ephrin B2 promotes cartilage destruction by osteoclasts in endochondral ossification

Stephen Tonna[1,2], Ingrid J. Poulton[1], Farzin Taykar[1], Patricia W. M. Ho[1], Brett Tonkin[1], Blessing Crimeen-Irwin[1], Liliana Tatarczuch[3], Narelle E. McGregor[1], Eleanor J. Mackie[3], T. John Martin[1,2] and Natalie A. Sims[1,2,*]

ABSTRACT

The majority of the skeleton arises by endochondral ossification, whereby cartilaginous templates expand and are resorbed by osteoclasts then replaced by osteoblastic bone formation. Ephrin B2 is a receptor tyrosine kinase expressed by osteoblasts and growth plate chondrocytes that promotes osteoblast differentiation and inhibits osteoclast formation. We investigated the role of ephrin B2 in endochondral ossification using Osx1Cre-targeted gene deletion. Neonatal *Osx1Cre.Efnb2*$^{\Delta/\Delta}$ mice exhibited a transient osteopetrosis demonstrated by increased trabecular bone volume with a high content of growth plate cartilage remnants and increased cortical thickness, but normal osteoclast numbers within the primary spongiosa. Osteoclasts at the growth plate had an abnormal morphology and expressed low levels of tartrate-resistant acid phosphatase; this was not observed in more mature bone. Electron microscopy revealed a lack of sealing zones and poor attachment of *Osx1Cre.Efnb2*$^{\Delta/\Delta}$ osteoclasts to growth plate cartilage. Osteoblasts at the growth plate were also poorly attached and impaired in their ability to deposit osteoid. By 6 months of age, trabecular bone mass, osteoclast morphology and osteoid deposition by *Osx1Cre.Efnb2*$^{\Delta/\Delta}$ osteoblasts were normal. Cultured chondrocytes from *Osx1Cre.Efnb2*$^{\Delta/\Delta}$ neonates showed impaired support of osteoclastogenesis but no significant change in *Rankl* (*Tnfsf11*) levels, whereas *Adamts4* levels were significantly reduced. A population of ADAMTS4^{+} early hypertrophic chondrocytes seen in controls was absent from *Osx1Cre.Efnb2*$^{\Delta/\Delta}$ neonates. This suggests that Osx1Cre-expressing cells, including hypertrophic chondrocytes, are dependent on ephrin B2 for their production of cartilage-degrading enzymes, including ADAMTS4, and this might be required for attachment of osteoclasts and osteoblasts to the cartilage surface during endochondral ossification.

KEY WORDS: Ephrin B2, Osteoclast, Chondrocyte, Osteoblast, Endochondral ossification, Sp7, Mouse

INTRODUCTION

Endochondral ossification is the process by which the majority of the skeleton develops. In this process, the cartilage model enlarges by chondrocyte proliferation, until it reaches a size where the central chondrocytes undergo hypertrophy. Two processes then take place: the periosteal bone collar is deposited by osteoblasts around the diaphysis (mid-shaft), and cartilage and hypertrophic chondrocytes are gradually destroyed by osteoclasts (bone-resorbing cells). The resulting cartilage remnants are gradually replaced with bone by repeated cycles of resorption by osteoclasts followed by osteoblastic bone formation; this process continues throughout skeletal growth. It has been suggested that mechanisms controlling osteoclast generation and activity at the growth plate may be distinct from those that exist on bone surfaces during adulthood (Poulton et al., 2012; Touaitahuata et al., 2014), but these remain poorly defined.

Ephrin B2 is a tyrosine kinase that is expressed in the skeleton in osteoblasts (bone-forming cells), matrix-embedded osteocytes and osteoclasts (Zhao et al., 2006; Allan et al., 2008). Its expression by osteoblasts is rapidly upregulated by parathyroid hormone (PTH) and the related protein (PTHrP; also known as PTHLH) (Allan et al., 2008). The interaction of ephrin B2 with Eph receptor B4 (EPHB4) restricts the ability of bone surface osteoblasts to support osteoclast formation (Takyar et al., 2013). This interaction also promotes osteoblast differentiation (Takyar et al., 2013) and prevents their apoptosis (Tonna et al., 2014). This is required for bone to be mineralised at the normal rate, thereby contributing to bone strength (Tonna et al., 2014) and, at least in part, mediating the anabolic effect of pharmacological PTH (Takyar et al., 2013; Tonna and Sims, 2014; Tonna et al., 2014).

Osteoblasts and chondrocytes are derived from a common precursor pool, and although it was originally thought that they are separate lineages, more recent studies indicate plasticity and transdifferentiation between these two cell types (Yang et al., 2014a, b; Zhou et al., 2014; Park et al., 2015). Both ephrin B2 and EPHB4 are detected in proliferating and hypertrophic chondrocytes at the growth plate (Wang et al., 2014), during fracture healing (Ito et al., 2006), in articular cartilage (Othman-Hassan et al., 2001), and in the ATDC5 chondrocyte cell line (Ito et al., 2006; Wang et al., 2014). At the growth plate, ephrin B2 and EPHB4 protein levels are reported to be lower in the absence of IGF1 (Wang et al., 2014), a factor that promotes chondrocyte proliferation during longitudinal bone growth downstream of growth hormone (Sims et al., 2000). Although pharmacological inhibition of ephrin B2/EPHB4 signalling in osteoblasts promoted RANKL (also known as TNFSF11) production and support of osteoclast formation (Takyar et al., 2013), the same reagent suppressed osteoclast formation when supported by chondrocytes (Wang et al., 2014). This latter effect appeared to be independent of RANKL production (Wang et al., 2014). This suggested that ephrin B2 regulates osteoclast formation by restraining the expression of RANKL in osteoblasts but promoting a RANKL-independent action that supports osteoclastogenesis in chondrocytes.

In this study, we targeted the deletion of ephrin B2 (*Efnb2*) to chondrocytes and osteoblasts in a mouse model (*Osx1Cre.Efnb2*$^{\Delta/\Delta}$), and found that these mice exhibit a neonatal osteopetrosis due to impaired osteoclastogenesis specifically at the growth plate. This points to a novel role for ephrin B2 in the chondrocyte that is required

[1]St Vincent's Institute of Medical Research, Fitzroy, Victoria 3065, Australia. [2]The University of Melbourne, Department of Medicine at St Vincent's Hospital, Fitzroy, Victoria 3065, Australia. [3]The University of Melbourne, Faculty of Veterinary and Agricultural Sciences, Parkville 3010, Australia.

*Author for correspondence (nsims@svi.edu.au)

Received 27 April 2015; Accepted 24 December 2015

Development (2016) 143, 648-657 doi:10.1242/dev.125625

for osteoclastogenesis and cartilage destruction during endochondral ossification.

RESULTS

Increased trabecular bone volume due to impaired osteoclast activity

von Kossa staining revealed substantially higher trabecular bone mass, including the presence of intact chondrocyte stacks (green boxes, Fig. 1A), in 2-day-old *Osx1Cre.Efnb2*$^{\Delta/\Delta}$ mice as compared with controls comprising wild-type mice (*Efnb2*$^{w/w}$), mice harbouring *Osx1Cre* but lacking the *Efnb2-loxP* transgene (*Osx1Cre.Efnb2*$^{w/w}$), and mice expressing two copies of the *Efnb2-loxP* transgene (*Efnb2*$^{f/f}$). Histomorphometric analysis (Fig. 1B) confirmed a significantly higher trabecular bone volume (BV/TV) and trabecular number (Tb.N) in *Osx1Cre.Efnb2*$^{\Delta/\Delta}$ femora compared with littermate controls, consistent with osteopetrosis (Fig. 1B). Trabecular thickness (Tb.Th) and trabecular separation were both significantly less than in controls. No significant effect of the *Osx1Cre* transgene on trabecular bone structure was detected. Similar observations were made in distal tibiae, proximal femur and distal femur (data not shown).

Osteopetrosis in *Osx1Cre.Efnb2*$^{\Delta/\Delta}$ neonatal mice was further indicated by Safranin O staining, which showed excessive cartilage remnants within the neonatal femoral diaphysis compared with *Efnb2*$^{f/f}$ littermates (Fig. 2A). There was also very little osteoid matrix on cartilage surfaces near the growth plate in *Osx1Cre.Efnb2*$^{\Delta/\Delta}$ (Fig. 2A). This is consistent with their low trabecular thickness, and suggests impaired osteoblast function. Although cartilage remnants within the trabecular bone were more abundant, the width of the hypertrophic zone was not significantly greater in neonatal *Osx1Cre.Efnb2*$^{\Delta/\Delta}$ mice compared with controls [mean hypertrophic zone width (μm)±s.e.m.: *Osx1Cre.Efnb2*$^{w/w}$, 120±8 (n=8); *Osx1Cre.Efnb2*$^{\Delta/\Delta}$, 156±20 (n=6); P=0.089].

Staining for the osteoclastic marker enzyme tartrate-resistant acid phosphatase (TRAP; also known as ACP5) of *Osx1Cre.Efnb2*$^{\Delta/\Delta}$ osteoclasts nearer to the growth plate revealed abnormal morphology and less intense TRAP staining compared with controls (Fig. 2B). When quantified at the chondro-osseous junction (Fig. 2C), the total number of osteoclasts was not significantly different between *Osx1Cre.Efnb2*$^{\Delta/\Delta}$ and *Efnb2*$^{f/f}$ controls, but most of the *Osx1Cre.Efnb2*$^{\Delta/\Delta}$ osteoclasts on the cartilage surface (chondroclasts) were small and rounded (<15 μm^2) (Fig. 2B,C). These small osteoclasts were not observed in sections from control mice, or in the *Osx1Cre.Efnb2*$^{\Delta/\Delta}$ metaphysis. On bone surfaces in this region, *Osx1Cre.Efnb2*$^{\Delta/\Delta}$ osteoclasts were of normal size and stained intensely for TRAP (Fig. 2C). This suggests altered osteoclast attachment or differentiation in *Osx1Cre.Efnb2*$^{\Delta/\Delta}$ mice specifically on cartilage surfaces at the growth plate.

Greater cortical thickness in neonatal *Osx1Cre.Efnb2*$^{\Delta/\Delta}$ mice

Analysis by microCT indicated increased material density and greater cortical thickness of the diaphyseal cortical bone in *Osx1Cre.Efnb2*$^{\Delta/\Delta}$ femora (Fig. 3A) compared with *Efnb2*$^{f/f}$ controls. When quantified, expression of the *Osx1Cre* transgene caused a significantly greater (15%) cortical thickness compared with non-Cre-expressing littermate controls (Fig. 3B). The *Osx1Cre.Efnb2*$^{\Delta/\Delta}$ mice showed a still greater cortical thickness than *Osx1Cre* transgenics (Fig. 3B), indicating either reduced resorption or greater bone formation in the diaphysis of these mice.

Defective osteoclast and osteoblast morphology visualised by electron microscopy

Electron microscopy of osteoclasts at the chondro-osseous junction confirmed their defective morphology (Fig. 4A,B). Osteoclasts from *Osx1Cre.Efnb2*$^{\Delta/\Delta}$ mice showed convoluted nuclear membranes and more heterochromatin than *Efnb2*$^{w/w}$, *Efnb2*$^{f/f}$ and *Osx1Cre.Efnb2*$^{w/w}$ osteoclasts (Fig. 4A,B). *Osx1Cre.Efnb2*$^{\Delta/\Delta}$ osteoclasts were smaller, and their contact with the cartilage matrix was less than that observed in *Efnb2*$^{w/w}$, *Efnb2*$^{f/f}$ and *Osx1Cre.Efnb2*$^{w/w}$ controls. Sealing zones and ruffled membranes, which form when osteoclasts attach to the bone surface and are required for acidification of the local environment and bone resorption, respectively, were readily observed in *Efnb2*$^{w/w}$, *Efnb2*$^{f/f}$ and *Osx1Cre.Efnb2*$^{w/w}$ (control) samples (Fig. 4B), but

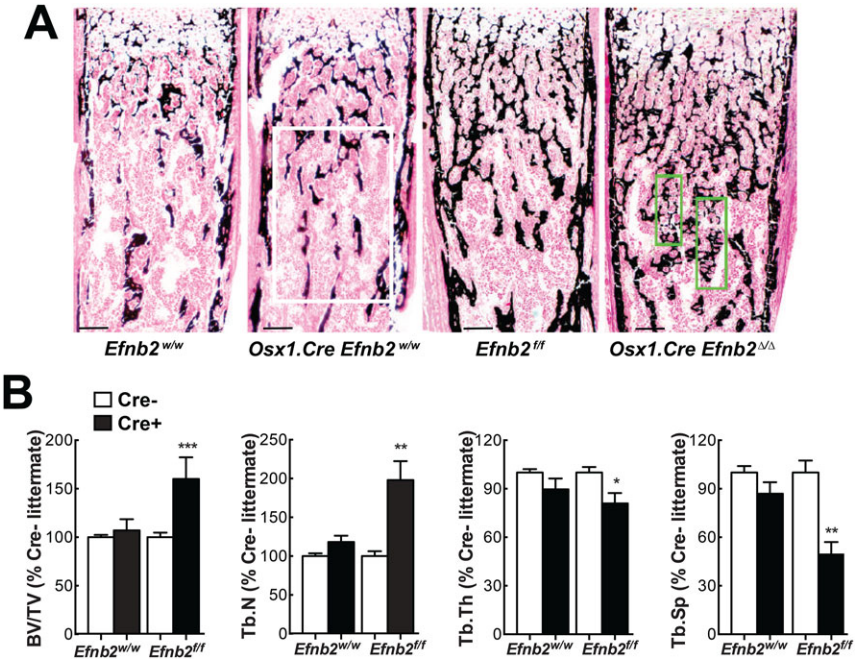

Fig. 1. Increased trabecular bone mass in neonatal *Osx1Cre.Efnb2*$^{\Delta/\Delta}$ mice. (A) von Kossa-stained images of the distal tibiae of 3.5-day-old *Osx1Cre.Efnb2*$^{\Delta/\Delta}$ mice (far right), littermate *Efnb2*$^{f/f}$ controls, and age-matched wild-type (*Efnb2*$^{w/w}$) and *Osx1Cre.Efnb2*$^{w/w}$ littermate controls. Green boxes indicate remnant chondrocyte stacks; the white box indicates the region used for histomorphometry. Scale bars: 50 μm.
(B) Histomorphometry of the distal tibiae. Trabecular bone volume (BV/TV), trabecular number (Tb.N), trabecular thickness (Tb.Th) and trabecular separation (Tb.Sp) were assessed in *Osx1Cre.Efnb2*$^{\Delta/\Delta}$ mice (far right bar), littermate *Efnb2*$^{f/f}$ controls, and age-matched *Efnb2*$^{w/w}$ and littermate *Osx1Cre.Efnb2*$^{w/w}$ mice at 2.5-3.5 days of age. Data are expressed as a percentage of values obtained in Cre-negative littermates calculated within each litter to account for slight differences in age; error bars indicate s.e.m. *P<0.05, **P<0.01, ***P<0.001 versus all controls. n=5 *Efnb2*$^{w/w}$, n=9 *Osx1Cre.Efnb2*$^{w/w}$, n=5 *Efnb2*$^{f/f}$ and n=6 *Osx1Cre.Efnb2*$^{f/f}$.

Development (2016) 143, 648-657 doi:10.1242/dev.125625

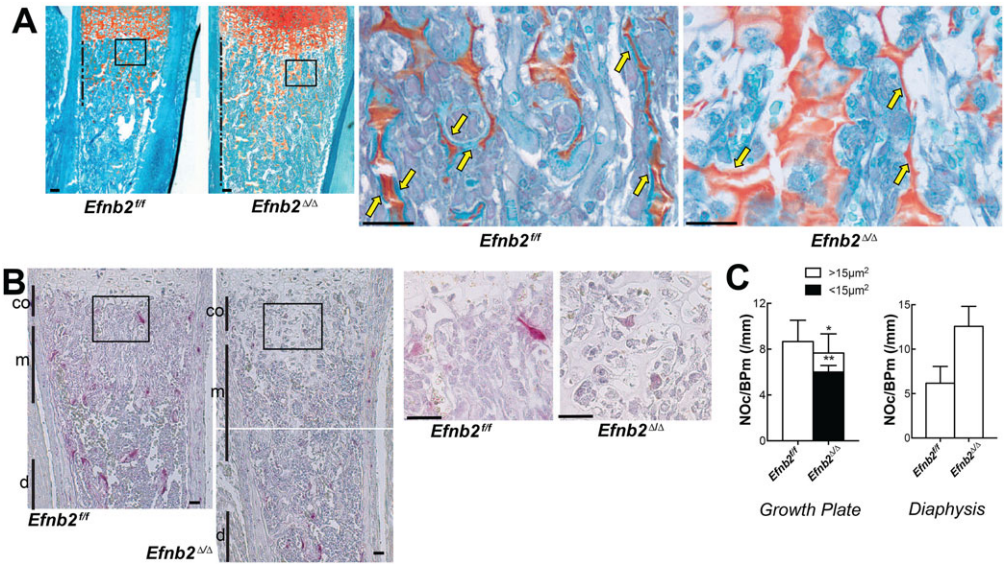

Fig. 2. Accumulation of cartilage remnants, lack of osteoid, and defective osteoclast formation at the chondro-osseous junction in *Osx1Cre.Efnb2*$^{\Delta/\Delta}$ mice. (A) Safranin O/Fast Green staining of femora from 3.5-day-old *Osx1Cre.Efnb2*$^{\Delta/\Delta}$ and *Efnb2*$^{f/f}$ littermates showing metaphyseal cartilage remnants (orange; extent marked with dashed line on the left) in *Osx1Cre.Efnb2*$^{\Delta/\Delta}$ femora. Boxes indicate approximate regions shown at high magnification on the right. Arrows indicate osteoid deposition (turquoise) on cartilage within the primary spongiosa in *Efnb2*$^{f/f}$ but a lack of osteoid in *Osx1Cre.Efnb2*$^{\Delta/\Delta}$ samples. (B) TRAP staining of 3.5-day-old *Osx1Cre.Efnb2*$^{\Delta/\Delta}$ and *Efnb2*$^{f/f}$ littermates indicates altered osteoclast morphology at the growth plate in *Osx1Cre.Efnb2*$^{\Delta/\Delta}$ samples. co, chondro-osseous junction; m, metaphysis; d, diaphysis. (C) Quantification of large (>15 μm^2) and small (<15 μm^2) TRAP-positive osteoclasts at the growth plate chondro-osseous junction and in the diaphysis of *Osx1Cre.Efnb2*$^{\Delta/\Delta}$ and *Efnb2*$^{f/f}$ littermates at 2.5-3.5 days of age. **P*<0.05 versus *Efnb2*$^{f/f}$ (large), ***P*<0.01 versus *Efnb2*$^{f/f}$ (small). *n*=6 *Efnb2*$^{w/w}$ and *n*=7 *Osx1Cre.Efnb2*$^{f/f}$. Scale bars: 50 μm.

were not detected in *Osx1Cre.Efnb2*$^{\Delta/\Delta}$ osteoclasts (Fig. 4B, right). This altered morphology is consistent with impaired resorption.

Osteoblast morphology was also notably different in *Osx1Cre.Efnb2*$^{\Delta/\Delta}$ mice compared with *Efnb2*$^{w/w}$, *Efnb2*$^{f/f}$ and *Osx1Cre.Efnb2*$^{w/w}$ controls (Fig. 4C). As previously observed in adult mice (Tonna et al., 2014), osteoblasts from neonatal *Osx1Cre.Efnb2*$^{\Delta/\Delta}$ mice displayed very little contact with each other or with the cartilage surface. Neonatal *Osx1Cre.Efnb2*$^{\Delta/\Delta}$ osteoblasts also displayed more heterochromatin, less endoplasmic reticulum and more apoptotic osteoblasts than controls, as previously observed (Tonna et al., 2014). All these features of osteoblasts in neonatal *Osx1Cre.Efnb2*$^{\Delta/\Delta}$ mice are consistent with impaired function, including the low level of osteoid deposition observed in the neonatal sections.

Reduced support of osteoclast formation by ephrin B2-deficient chondrocytes

To determine whether the impaired osteoclast formation in *Osx1Cre.Efnb2*$^{\Delta/\Delta}$ mice resulted from reduced chondrocytic support of osteoclast formation, we co-cultured *Osx1Cre.Efnb2*$^{\Delta/\Delta}$ chondrocytes with osteoclast precursors from C57BL/6 mice and treated them with 1,25-dihydroxyvitamin D_3 to stimulate osteoclast formation. *Osx1Cre.Efnb2*$^{\Delta/\Delta}$ chondrocytes showed a reduced capacity to support osteoclast formation compared with control *Efnb2*$^{f/f}$ chondrocytes (Fig. 5A), consistent with the defective osteoclast formation observed at the chondro-osseous junction *in vivo*.

Altered differentiation of *Osx1Cre.Efnb2*$^{\Delta/\Delta}$ chondrocytes

Osx1Cre.Efnb2$^{\Delta/\Delta}$ chondrocytes showed normal *Efnb2* mRNA levels at day 7, but, consistent with increased osterix (*Sp7*) expression at day 21, *Efnb2* mRNA levels at day 21 were significantly lower in *Osx1Cre.Efnb2*$^{\Delta/\Delta}$ than in *Efnb2*$^{f/f}$ chondrocytes (Fig. 5B), consistent with previous reports of *Osx1Cre* expression in these cells (Rodda and McMahon, 2006; Maes et al., 2010; Chen et al., 2014). *Osx1Cre.Efnb2*$^{\Delta/\Delta}$ chondrocytes also showed significantly higher *Col10a1* but lower osteopontin (*Spp1*) mRNA levels at day 21 compared with the *Efnb2*$^{f/f}$ control, suggesting an alteration in the normal pattern of chondrocytic gene expression in *Efnb2*-deficient chondrocytes in

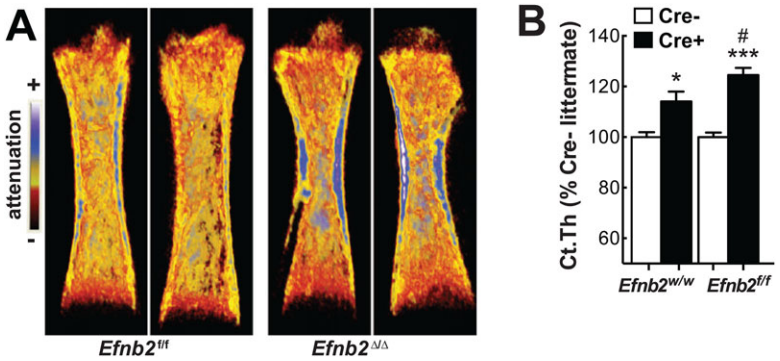

Fig. 3. Increased cortical thickness in *Osx1Cre.Efnb2*$^{\Delta/\Delta}$ mice. (A) Images showing X-ray attenuation of 3.5-day-old *Efnb2*$^{f/f}$ and *Osx1Cre.Efnb2*$^{\Delta/\Delta}$ littermates (two per genotype). The scale on the left shows the X-ray attenuation gradient. (B) Mean cortical thickness (Ct.Th) of *Osx1Cre.Efnb2*$^{\Delta/\Delta}$ mice (far right bar), littermate *Efnb2*$^{f/f}$ controls, and age-matched *Efnb2*$^{w/w}$ and littermate *Osx1Cre.Efnb2*$^{w/w}$ mice at 2.5-3.5 days of age. Data are the mean percentage of Cre-negative littermate Ct.Th; error bars indicate s.e.m. **P*<0.05, ****P*<0.001 versus Cre-negative control; $^{\#}$*P*<0.05 versus *Osx1Cre.Efnb2*$^{w/w}$. *n*=6 *Efnb2*$^{w/w}$, *n*=9 *Osx1Cre.Efnb2*$^{w/w}$, *n*=9 *Efnb2*$^{f/f}$ and *n*=6 *Osx1Cre.Efnb2*$^{f/f}$.

Development (2016) 143, 648-657 doi:10.1242/dev.125625

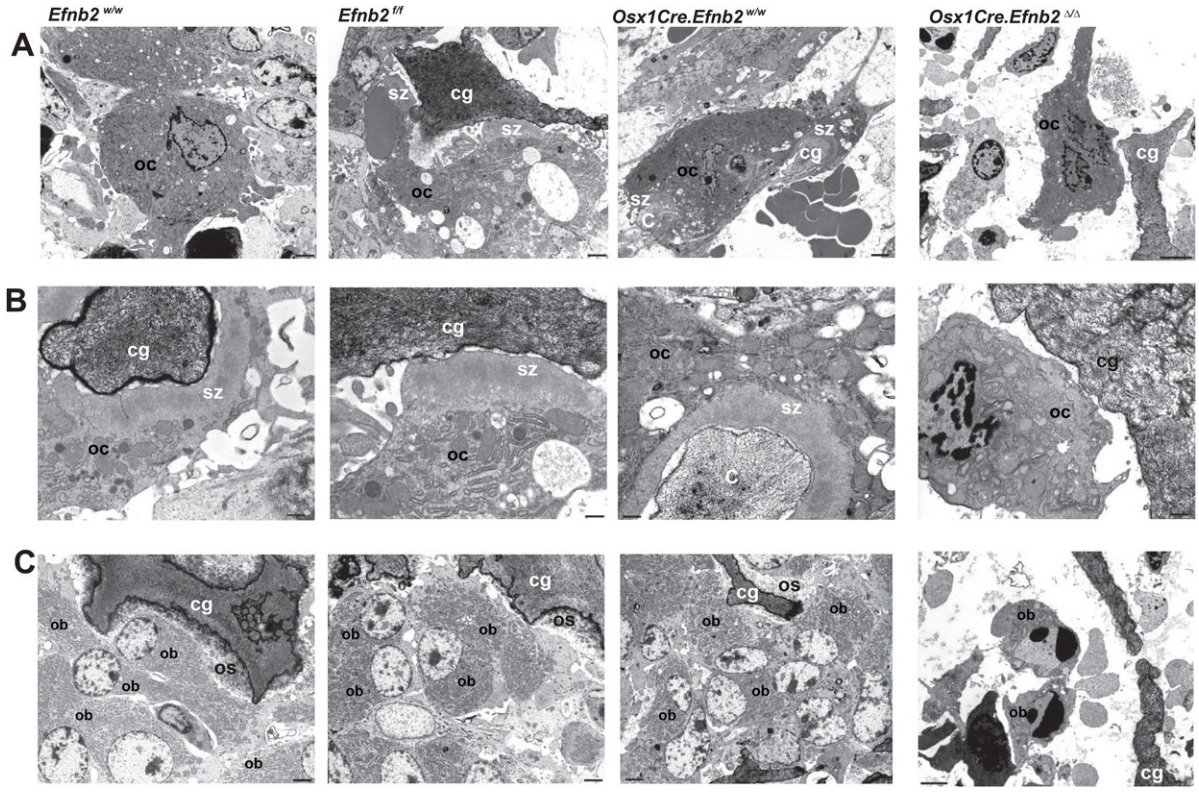

Fig. 4. Altered osteoclast and osteoblast attachment to cartilage in *Osx1Cre.Efnb2*$^{\Delta/\Delta}$ mice. Electron microscopy images from neonatal controls (*Efnb2*$^{w/w}$, *Efnb2*$^{f/f}$ and *Osx1Cre.Efnb2*$^{w/w}$) showing osteoclasts (oc) and their sealing zones (sz) abutting cartilage matrix (cg) (A,B), and osteoblasts (ob) with abundant intercellular attachment and attachment to osteoid (os) on the cartilage surface (C). By contrast (far right), neonatal *Osx1Cre.Efnb2*$^{\Delta/\Delta}$ samples (littermates to *Osx1Cre.Efnb2*$^{w/w}$) show osteoclasts adjacent to cartilage, their lack of sealing zones, and apoptotic osteoblasts not attached to the bone surface. Scale bars: 1.9 µm in A; 3.3 µm in B; 0.5 µm in C.

culture. There was no significant alteration in the mRNA levels of *Rankl* (*Tnfsf11*) or its decoy receptor *Opg* (*Tnfrsf11b*) (Fig. 5B).

Hypertrophic chondrocytes also promote the destruction of growth plate cartilage by expression of a number of catabolic enzymes, including the matrix metalloproteinases (MMPs) MMP13 (Johansson et al., 1997) and MMP9 (Shinoda et al., 2008; Golovchenko et al., 2013) and the aggrecanases ADAMTS4 and ADAMTS5 (Glasson et al., 2004; Rogerson et al., 2008). We reasoned that, since ephrin B2 deletion was targeted to osteoblasts and chondrocytes, the lack of cartilage destruction in *Osx1Cre.Efnb2*$^{\Delta/\Delta}$ mice might relate to reduced production of these proteins by hypertrophic chondrocytes. Whereas no changes in *Mmp13*, *Mmp9* or *Adamts5* mRNA were detected (Fig. 5B; data not shown), *Adamts4* levels were ∼50% lower in *Osx1Cre.Efnb2*$^{\Delta/\Delta}$ cultured chondrocytes at 21 days compared with control (Fig. 5B).

Immunohistochemical staining for ADAMTS4 showed strong staining in resting chondrocytes and osteoblasts in both *Osx1Cre.Efnb2*$^{\Delta/\Delta}$ and *Efnb2*$^{f/f}$ femora and tibiae (distal tibiae shown in Fig. 6A,B). A similar proportion of resting chondrocytes stained positively for ADAMTS4 (Fig. 6C,D), and in both *Osx1Cre.Efnb2*$^{\Delta/\Delta}$ and *Efnb2*$^{f/f}$ femora and tibiae ADAMTS4 was not detected in proliferating chondrocytes. The pattern of ADAMTS4 staining differed in more mature chondrocytes. In *Efnb2*$^{f/f}$ growth plates, early hypertrophic chondrocytes showed positive intracellular staining for ADAMTS4, whereas late hypertrophic chondrocytes showed little to no stain (Fig. 6E). However, in *Osx1Cre.Efnb2*$^{\Delta/\Delta}$ growth plates no ADAMTS4 staining was detected in early hypertrophic chondrocytes, and very few late hypertrophic chondrocytes were positive for this antigen. ADAMTS4 was only detected in those hypertrophic chondrocytes located at the chondro-osseous junction in *Osx1Cre.Efnb2*$^{\Delta/\Delta}$ growth plates (Fig. 6F). IgG control sections were clear of staining (Fig. 6G).

Resolution of the osteopetrotic phenotype by 6 weeks of age

We previously reported that 12-week-old *Osx1Cre.Efnb2*$^{\Delta/\Delta}$ mice do not exhibit osteopetrosis, suggesting resolution of this phenotype. To determine when this transition occurs, we assessed whether the neonatal osteopetrosis of *Osx1Cre.Efnb2*$^{\Delta/\Delta}$ mice was detectable at 6 weeks of age. MicroCT and histomorphometric analysis of *Osx1Cre.Efnb2*$^{\Delta/\Delta}$ and *Osx1Cre.Efnb2*$^{f/f}$ mice at 6 weeks of age revealed no significant differences in trabecular structure or in the numbers of osteoclasts (NOc/BPm) or osteoblasts (NOb/BPm), nor was there any detectable difference in the abundance of cartilage remnants (Table 1). As observed at 12 weeks, the mineral appositional rate was significantly reduced (Table 1), confirming this functional defect in bone mineralisation. Consistent with the resolution of osteopetrosis, no differences were observed in the width of the growth plate [mean growth plate width (µm)±s.e.m. (n=6-9/group): *Osx1Cre.Efnb2*$^{\Delta/\Delta}$, 117±9; *Osx1Cre.Efnb2*$^{w/w}$, 109±6], nor of the proliferating or hypertrophic zones [proportion of hypertrophic zone to proliferating zone (%±s.e.m.): *Osx1Cre.Efnb2*$^{\Delta/\Delta}$, 46.7±6.4; *Osx1Cre.Efnb2*$^{w/w}$, 43.5±4.9] at 6 weeks of age$^{w/w}$. Surprisingly, although the osteopetrosis was rescued by this stage of growth, osteoclasts at the chondro-osseous junction still displayed a defective morphology as visualised by electron microscopy (data not shown), further indicating that the defective support of osteoclastogenesis was specific to the growth plate region. At 6 weeks of age, osteoblast

Development (2016) 143, 648-657 doi:10.1242/dev.125625

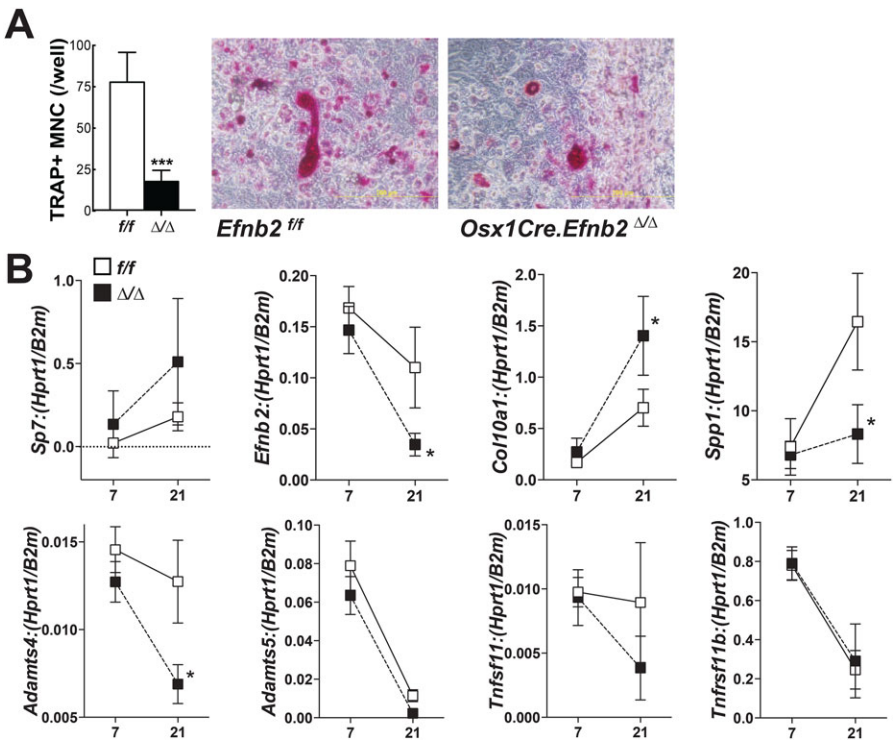

Fig. 5. *Osx1Cre.Efnb2*$^{Δ/Δ}$ chondrocytes exhibit less support of osteoclastogenesis and altered gene expression, including low *Adamts4*. (A) Osteoclasts [TRAP^{+} were multinucleated cells (MNC)] generated from C57BL/6 bone marrow macrophages cultured with differentiated *Efnb2*$^{f/f}$ and *Osx1Cre.Efnb2*$^{Δ/Δ}$ primary chondrocytes and treated with 1,25-dihydroxyvitamin D_3. Data are mean±s.e.m. from three independent cultures. (B) Gene expression of *Efnb2*$^{f/f}$ and *Osx1Cre.Efnb2*$^{Δ/Δ}$ primary chondrocytes at days 7 and 21 of differentiation. Shown are osterix (*Sp7*), ephrin B2 (*Efnb2*), collagen X (*Col10a1*), osteopontin (*Spp1*), *Adamts4*, *Adamts5*, *Rankl* (*Tnfsf11*) and *Opg* (*Tnfrsf11b*). Data are the mean±s.e.m. of the ratio to the geometric mean of *Hprt1* and *B2m* from three biological replicates. *P<0.05, ***P<0.001 versus Cre-negative *Efnb2*$^{f/f}$ cells at the same time point (genotype effect).

morphology was partially recovered compared with control mice, with osteoblasts showing improved attachment to each other; attachment to bone surfaces was still impaired, some osteoblasts showed distended endoplasmic reticulum, and more apoptotic osteoblasts were observed than usual, as previously reported in 9- and 12-week-old mice (Tonna et al., 2014).

DISCUSSION

This work reveals a novel and necessary function for ephrin B2 signalling in chondrocytes during bone development. The data suggest that ephrin B2 expression by hypertrophic chondrocytes is required for their expression of genes that promote cartilage degradation, such as *Adamts4*. This preparation of the cartilage matrix might promote the attachment and activity of osteoclasts, which resorb cartilage matrix, and osteoblasts, which form bone on cartilage remnants *in vivo*. Such a mechanism of cartilage matrix-mediated control of osteoclast attachment might be involved in transient forms of osteopetrosis in the neonatal skeleton and might regulate endochondral fracture healing.

Neonatal *Osx1Cre.Efnb2*$^{Δ/Δ}$ mice exhibited a significant osteopetrosis that was most notable in the first few days after birth. While chondrocyte morphology appeared normal, the

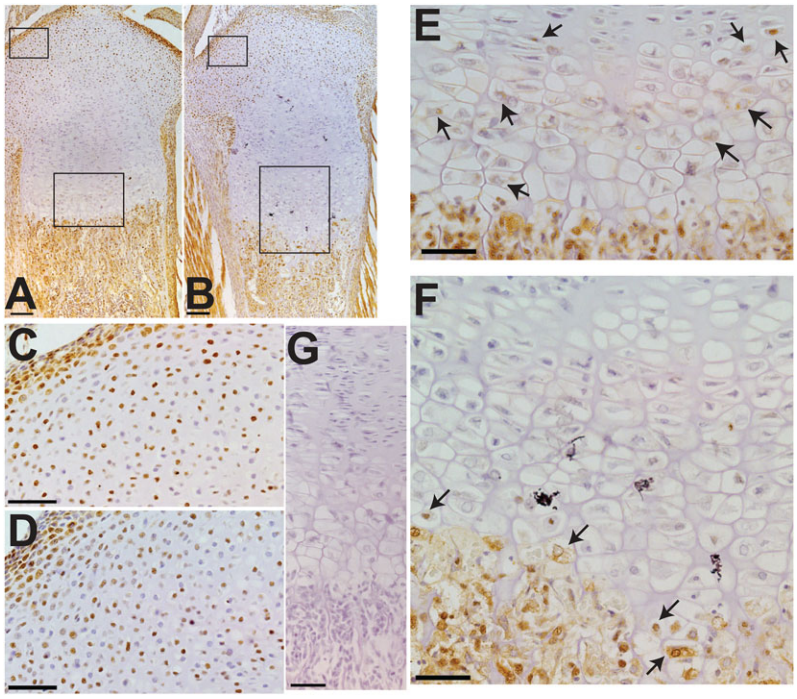

Fig. 6. ADAMTS4 immunohistochemistry in neonatal *Efnb2*$^{f/f}$ and *Osx1Cre.Efnb2*$^{Δ/Δ}$ proximal tibiae. (A,C,E,G) *Efnb2*$^{f/f}$; (B,D,F) *Osx1Cre.Efnb2*$^{Δ/Δ}$. (A,B) Low magnification images showing the overall staining pattern and the regions selected for high magnification. (C,D) Higher magnification images of the upper boxes in A and B, respectively, showing resting and articular chondrocytes. (E,F) Higher magnification images of the lower boxes in A and B, respectively, showing of the base of the proliferating zone through to the chondro-osseous junction. Examples of stained cells are indicated with arrows. (G) IgG control section of an *Efnb2*$^{f/f}$ femur showing the base of the proliferating zone through to the chondro-osseous junction. Scale bars: 100 µm in A,B; 50 µm in C-G.

Development (2016) 143, 648-657 doi:10.1242/dev.125625

Table 1. Structural and histomorphometric analysis of female 6-week-old *Osx1Cre.Efnb2*$^{\Delta/\Delta}$ and *Osx1Cre.Efnb2*$^{w/w}$ littermates

	MicroCT (femur)							
	BV/TV (%)	Tb.N (/mm)	Tb.Th (μm)	Tb.Sp (μm)	Ct.Th (μm)	Ec.Ci (mm)	Ps.Ci (mm)	MoI (mm^4)
Osx1Cre.Efnb2$^{w/w}$	12.8±0.9	2.18±0.14	58.3±0.5	267.5±23.6	140.2±3.3	1.82±0.03	5.87±0.16	0.229±0.013
Osx1Cre.Efnb2$^{\Delta/\Delta}$	13.0±0.8	2.27±0.12	57.2±0.6	234.5±10.8	124.9±3.3**	1.77±0.02	5.51±0.07*	0.189±0.010**
	Histomorphometry (tibia) – osteoblasts and bone formation							
	OV/BV (%)	OTh (μm)	OS/BS (%)	ObS/BS (%)	NOb/BPm (/mm)	MAR (μm/day)	MS/BS (%)	BFR/BV (%/day)
Osx1Cre.Efnb2$^{w/w}$	3.80±0.68	3.23±0.72	17.5±3.3	22.8±4.7	14.7±2.7	2.50±0.11	36.5±5.0	6.67±0.54
Osx1Cre.Efnb2$^{\Delta/\Delta}$	3.33±0.65	2.76±0.21	17.5±2.6	22.9±3.5	13.6±2.1	1.89±2.10**	41.9±3.9	5.76±0.47
	Histomorphometry (tibia) – osteoclasts							
	OcS/BS (%)	NOc/BPm (/mm)	CtgV/BV (%)					
Osx1Cre.Efnb2$^{w/w}$	16.0±3.4	3.18±0.60	7.17±3.23					
Osx1Cre.Efnb2$^{\Delta/\Delta}$	18.7±2.0	3.85±0.47	8.81±1.14					

Shown are histomorphometry data for the proximal tibiae and microCT of the distal femur: trabecular bone volume (BV/TV), trabecular number (Tb.N), trabecular thickness (Tb.Th), trabecular separation (Tb.Sp), cortical thickness (Ct.Th), endocortical circumference (Ec.Ci), periosteal circumference (Ps.Ci), moment of inertia (MoI), osteoid volume/bone volume (OV/BV), osteoid thickness (OTh), osteoid surface/bone surface (OS/BS), osteoblast surface/bone surface (ObS/BS), osteoblast number per unit bone perimeter (NOb/BPm), mineral appositional rate (MAR), mineralising surface/bone surface (MS/BS), bone formation rate/bone volume (BFR/BV), osteoclast surface/bone surface (OcS/BS), osteoclast number per unit bone perimeter (NOc/BPm), volume of cartilage remnants within the trabecular bone (CtgV/BV); n=6-12/group, mean±s.e.m. *, P<0.05, **, P<0.01 vs *Osx1Cre.Efnb2*$^{w/w}$.

destruction of calcified matrix surrounding hypertrophic chondrocytes was delayed. Impaired destruction of cartilage during endochondral ossification is a hallmark of osteopetrosis, regardless of whether it is caused by impaired osteoclast formation or a defect in osteoclast function (Del Fattore et al., 2008). The combination of a high level of cartilage remnants in the presence of normal osteoclast numbers, as seen in the *Osx1Cre.Efnb2*$^{\Delta/\Delta}$ mice, is similar to what has been observed in mice in which osteoclast function is impaired, either due to poor acidification or low enzyme activity, such as in *Acp5* (TRAP) (Hayman et al., 1996), *Atp6i* (*Tcirg1*) (Li et al., 1999) or *Clc7* (*Clcn7*) (Neutzsky-Wulff et al., 2010) null mice, or when osteoclast attachment is disrupted, as in *Src* (Soriano et al., 1991) and *Pyk2* (*Ptk2b*) (Gil-Henn et al., 2007) null mice. Cartilage remnants within trabecular bone are also observed in humans with osteopetrosis due to defective osteoclast function (Blair et al., 2009). Since osteoclast number was normal in *Osx1Cre.Efnb2*$^{\Delta/\Delta}$ mice, we suggest that ephrin B2 expression in *Osx1Cre*-expressing cells is required for the normal function of osteoclasts at the developing growth plate.

Defective osteoclast function in these mice was a surprising observation since *Efnb2* gene recombination was directed with *Osx1Cre*, which targets the osteoblast lineage and prehypertrophic and hypertrophic chondrocytes (Rodda and McMahon, 2006; Maes et al., 2010). In these mice, *Efnb2* mRNA levels were reduced in osteoblasts (Tonna et al., 2014) and chondrocytes (current work), and we previously confirmed that *Efnb2* mRNA levels are not altered in osteoclast precursors or differentiated osteoclasts generated from *Osx1Cre.Efnb2*$^{\Delta/\Delta}$ mice (Tonna et al., 2014). This suggests that osteoblasts or chondrocytes that lack ephrin B2 may lack some mechanism of supporting osteoclast activity, particularly near the growth plate. Since the bone matrix is appropriately resorbed as the mice age, we suggest that the defect rests within the mineralised cartilage deposited by ephrin B2-deficient chondrocytes.

Osteoblast attachment observed by electron microscopy of the cartilage remnants was defective in *Osx1Cre.Efnb2*$^{\Delta/\Delta}$ mice in neonatal bone, as we previously observed in adults (Tonna et al., 2014). In remodelling trabecular bone, which was assessed in adult *Osx1Cre.Efnb2*$^{\Delta/\Delta}$ mice, osteoid volume was significantly increased due to delayed mineralisation (Tonna et al., 2014). By contrast, in the neonatal growth plate, where osteoblasts attach to and form osteoid on a cartilage template, *Osx1Cre.Efnb2*$^{\Delta/\Delta}$ osteoblasts showed defective osteoid deposition (Fig. 6). This suggests that the same changes in cartilage composition that impair osteoclast attachment in this region may also impair the attachment and function of osteoblasts. By contrast, during bone remodelling in adult *Osx1Cre.Efnb2*$^{\Delta/\Delta}$ mice, osteoblasts work on a bone surface to which they are capable of attaching (Fig. 6); it is their maturation to late stages, including osteocytes, that leads to defective mineralisation of the osteoid, as observed both at 6 and 12 weeks of age.

To determine how chondrocytes support cartilage destruction, we focused on two possible activities: the support of osteoclast formation by *Efnb2*-deficient chondrocytes, and their expression of cartilage-degrading enzymes. Co-culture of differentiated primary chondrocytes from *Osx1Cre.Efnb2*$^{\Delta/\Delta}$ mice showed impaired support of osteoclast formation, as we previously observed with osteoblasts derived from mice of the same genotype (Tonna et al., 2014). This was also consistent with the work of others showing that specific inhibition of the ephrin B2-EPHB4 interaction with the TNYL-RAW peptide inhibited osteoclast formation supported by the ATDC5 chondrocyte cell line (Wang et al., 2014). Surprisingly, mRNA levels for RANKL, a ligand that supports osteoclast formation and is expressed by hypertrophic chondrocytes (Kartsogiannis et al., 1999), and for the RANKL decoy receptor OPG were unchanged. This supports a model whereby the ephrin B2/EPHB4 role in chondrocytic support of osteoclastogenesis is independent of the RANKL/OPG system, as previously suggested (Wang et al., 2014). We hypothesized that enzymatic degradation of the cartilage matrix may also play a role in the osteoclastic destruction of cartilage surrounding hypertrophic chondrocytes.

Chondrocytes from the *Osx1Cre.Efnb2*$^{\Delta/\Delta}$ mice exhibited a number of changes in gene expression and an altered pattern of ADAMTS4 staining. Collagen X and osteopontin levels normally increase with chondrocyte hypertrophy (Lian et al., 1993), but their co-regulation was disrupted in *Osx1Cre.Efnb2*$^{\Delta/\Delta}$ chondrocytes: *Col10a1* levels were elevated but osteopontin levels were reduced, suggesting disruption of the normal profile of hypertrophic gene expression. Since *Adamts4* is upregulated in hypertrophic chondrocytes (Lian et al., 1993; Glasson et al., 2004), the low level of *Adamts4* mRNA that we observe in *Osx1Cre.Efnb2*$^{\Delta/\Delta}$ chondrocytes is more likely to reflect a delay in chondrocyte

Development (2016) 143, 648-657 doi:10.1242/dev.125625

hypertrophy in the absence of ephrin B2 than direct regulation by osteopontin, particularly since exogenous treatment with this protein is reported to suppress *Adamts4* expression (Gao et al., 2015). A full understanding of the changes in gene expression in *Osx1Cre.Efnb2*$^{\Delta/\Delta}$ chondrocytes would require a non-biased approach, such as a microarray study of micro-dissected mRNA from these mutant growth plates.

Hypertrophic chondrocytes also express metalloproteinases and aggrecanases (Johansson et al., 1997; Glasson et al., 2004; Shinoda et al., 2008; Golovchenko et al., 2013) and there are several lines of evidence indicating that these regulate osteoclast activity during endochondral ossification. Mice carrying a collagen mutation rendering it resistant to collagenases show impaired osteoclastic resorption of growth plate cartilage (Chiusaroli et al., 2003), while *Mmp13* null mice show impaired osteoclast attachment in endochondral fracture healing (Holliday et al., 1997; Kosaki et al., 2007). ADAMTS4 has previously been detected in hypertrophic chondrocytes at the growth plate of adult mice (Glasson et al., 2004), in osteoblasts in developing limbs (Nakamura et al., 2005) and is elevated during endochondral fracture healing (Wang et al., 2006). Our detection of ADAMTS4 in ∼60% of resting chondrocytes and in early hypertrophic chondrocytes suggests that it may play a role in degradation of the cartilage matrix during neonatal bone development.

In cultured ephrin B2-deficient chondrocytes we observed significantly lower *Adamts4* mRNA levels compared with control cells at day 21 of differentiation. Although ADAMTS4 immunohistochemical staining was strong in osteoblasts and in a proportion of resting chondrocytes in *Osx1Cre.Efnb2*$^{\Delta/\Delta}$ limbs, no clear ADAMTS4 staining was detected in early hypertrophic chondrocytes. By contrast, only hypertrophic chondrocytes at the chondro-osseous junction were positive for ADAMTS4. This provides another indication of altered chondrocyte differentiation, and suggests that delayed ADAMTS4 expression may play a role in the impaired cartilage degradation/resorption in the absence of ephrin B2. Although mice deficient in *Adamts4* have previously been reported to have no gross developmental defect (Glasson et al., 2004), a phenotype such as that we describe here in *Osx1Cre.Efnb2*$^{\Delta/\Delta}$ mice would not be detected by a screen for gross morphological changes.

Our findings suggest that cartilage degradation by chondrocytes is required to prepare the cartilage matrix for osteoclast attachment and resorptive activity. This is consistent with similar activities in bone, where collagenase prepares bone surfaces for osteoclastic attachment and subsequent resorption (Chambers et al., 1985; Chambers and Fuller, 1985). Several outcomes of this action have been proposed: first, that osteoclasts attach more strongly to degraded collagen matrix; second, that fragments of degraded collagen 'activate' osteoclasts to resorb bone (Holliday et al., 1997). We suggest that similar mechanisms, initiated by chondrocytic enzyme production, may play a similar role to mediate osteoclast attachment to growth plate cartilage in the hypertrophic zone.

The osteopetrosis of neonatal *Osx1Cre.Efnb2*$^{\Delta/\Delta}$ mice had fully resolved by 6 weeks of age, consistent with our previous observation that 12-week-old *Osx1Cre.Efnb2*$^{\Delta/\Delta}$ mice have normal trabecular bone mass (Tonna et al., 2014). Osteopetrosis varies widely in its aetiology, and forms that resolve before puberty have been described in rats and human (Marks, 1973; Monaghan et al., 1991; Cielinski and Marks, 1995; Del Fattore et al., 2008), although no mechanism for this spontaneous resolution is known. One common element of these self-resolving forms of osteopetrosis is a defect in osteoclast enzyme function. The low level of TRAP staining observed in *Osx1Cre.Efnb2*$^{\Delta/\Delta}$ osteoclasts on cartilage is consistent with this, and the altered osteoclast morphology is strikingly similar to observations made in the transient osteopetrosis of the microphthalmia rat model (Cielinski and Marks, 1994). Notably, TRAP staining in the diaphysis, where osteoclasts attach to bone, was normal, consistent with previous observations in adult mice (Tonna et al., 2014). Thus, the resolution of transient osteopetrosis in humans and other mammals might be explained by the lesser contribution of resorption of growth plate cartilage to trabecular bone mass with age, as longitudinal growth declines.

The contrast between the normal trabecular bone mass at 6 weeks and the development of a high-bone-mass phenotype in female *Osx1Cre.Efnb2*$^{\Delta/\Delta}$ mice at 26 weeks of age (Tonna et al., 2014) is also likely to relate to altered contributions of endochondral ossification and bone remodelling to trabecular bone mass with age (Fig. 7). Trabecular bone mass in neonatal mice reflects the process of endochondral ossification, where resorption of cartilage templates is necessary for subsequent osteoblast-mediated bone formation. Impaired osteoclast activity at this age leads to osteopetrosis, characterised by high trabecular number but low trabecular thickness. In the adult mouse, as well as the contribution of endochondral ossification to bone mass being lower, trabecular bone mass is measured in the secondary spongiosa. This region does not exist in the neonatal mouse, and its trabecular bone volume depends on the balance between bone formation by osteoblasts and bone resorption by osteoclasts. During the transition period (6 and 12 weeks of age), both endochondral ossification and remodelling contribute to bone mass. We suggest that, in the *Osx1Cre.Efnb2*$^{\Delta/\Delta}$ mice, the low level of osteoid deposition on the cartilage template leads to normal trabecular bone mass by 6 weeks of age. In the secondary spongiosa of 12-week-old *Osx1Cre.Efnb2*$^{\Delta/\Delta}$ mice, osteoclast numbers are low and bone mineralisation is delayed, with a slight imbalance leading to a gradual accumulation of bone mass in this region that is not detected until 26 weeks of age. A phenotype with different effects on bone mass in the primary versus the secondary spongiosa, due to different control mechanisms in these regions, has been reported previously (Poulton et al., 2012).

Another region in which the bone phenotype differed significantly between the adult and neonatal mouse was the cortical bone. Neonatal *Osx1Cre.Efnb2*$^{\Delta/\Delta}$ mice showed thicker cortical bone than their control littermates, but by 6 weeks of age the cortical thickness was low due to impaired periosteal expansion. The latter finding is consistent with our previous observations in older adult mice (Tonna et al., 2014). During bone development the cortical bone forms and narrows as osteoclasts resorb cartilage from the centre of the anlagen. Impaired osteoclast activity, as observed in neonatal *Osx1Cre.Efnb2*$^{\Delta/\Delta}$ mice, results in a lack of resorption of the primary ossification centre and a delay in the reduction of cortical width. As the mice age, cortical bone thickens through periosteal growth, a process that is impaired in *Osx1Cre.Efnb2*$^{\Delta/\Delta}$ mice. As in the trabecular bone, cortical bone development and cortical expansion are differently affected by the deletion of ephrin B2 in osteoblasts and chondrocytes.

Ephrin B2 is thought to depend on cell-cell contact for signalling (Pasquale, 2010). Although extensive cell-cell contact exists within the osteocyte network (Buenzli and Sims, 2015) and between bone-forming osteoblasts, and contact-dependent mechanisms are recognised to control bone formation (Tonna and Sims, 2014), it is not clear how membrane-bound ephrin B2 could influence cell function in chondrocytes since these cells are isolated from each other by the cartilaginous matrix. There are two possibilities: ephrin B2 might be capable of autocrine signalling through EPHB4, which is also expressed by hypertrophic chondrocytes (Wang et al., 2014);

Development (2016) 143, 648-657 doi:10.1242/dev.125625

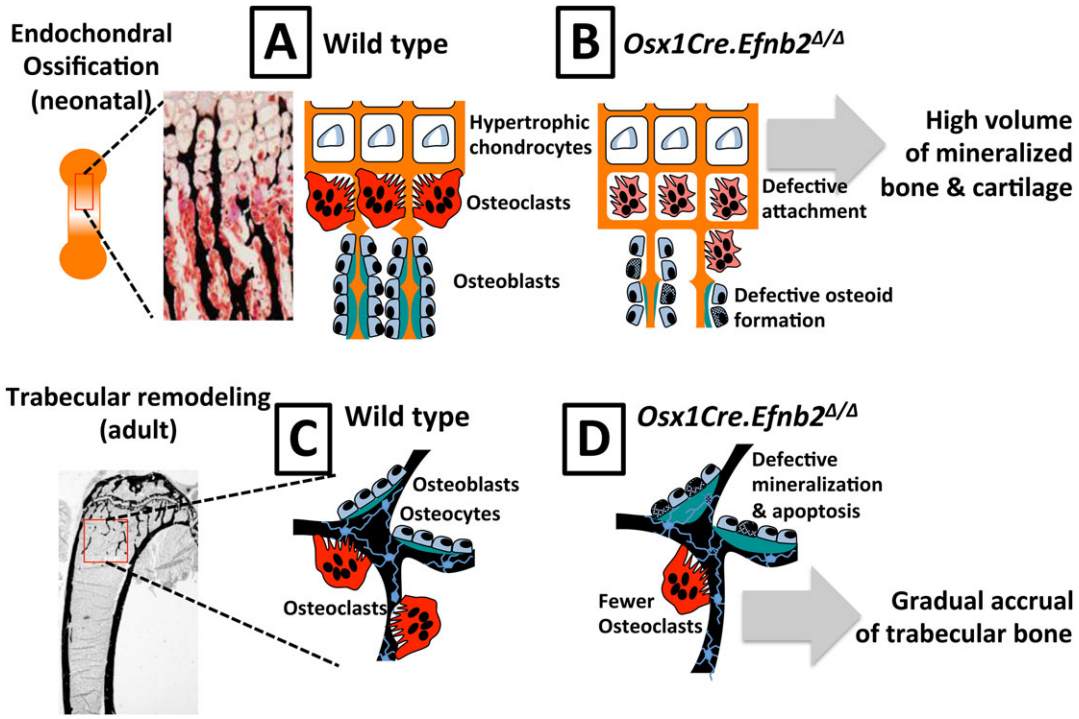

Fig. 7. Phenotypic differences between neonatal and adult *Osx1Cre.Efnb2*$^{\Delta/\Delta}$ mice. (A) In neonatal mice, osteoclasts resorb cartilage (orange) surrounding the hypertrophic chondrocytes, and osteoblasts lay down new osteoid on template that remains for the trabecular network. (B) In neonatal *Osx1Cre.Efnb2*$^{\Delta/\Delta}$ mice, osteoclast and osteoblast attachment to the cartilage surface is defective. Defective osteoclast activity leads to an increase in cartilage remnants and a high volume of mineralised bone and cartilage. In addition, owing to poor osteoblast attachment and apoptosis (shaded cells), very little osteoid is deposited. (C) In trabecular remodelling – a process that occurs in the secondary spongiosa (red box) – osteoclast and osteoblast activities determine trabecular structure. (D) In adult *Osx1Cre.Efnb2*$^{\Delta/\Delta}$ mice there are fewer osteoclasts. This lack of resorption, and defective mineralisation caused by osteoblast and osteocyte apoptosis (shaded cells), were associated with a gradual accumulation of trabecular bone.

alternatively, there might be cell-cell contact between hypertrophic chondrocytes. However, although prehypertrophic chondrocytes express the gap junction components connexin 43 (Gja1) and pannexin 3 (Schwab et al., 1998; Iwamoto et al., 2010; Bond et al., 2011), gap junctions between growth plate chondrocytes have not been observed *in situ*.

In conclusion, *Osx1Cre*-targeted deletion of ephrin B2 results in a transient neonatal osteopetrosis caused by a region-specific defect in osteoclast attachment and activity. This points to a role for cartilage-specific factors, including ADAMTS4, in controlling osteoclastic resorption during endochondral bone development.

MATERIALS AND METHODS

Animals

Animal procedures were approved by the St Vincent's Health Melbourne Animal Ethics Committee. *Tg(Sp7-tTA,tetO-EGFP/cre)*^{1Amc} *(Osx1-GFP::Cre)* mice backcrossed onto C57BL/6 were generated as previously described (Tonna et al., 2014) by crossing *Tg(Sp7-tTA,tetO-EGFP/cre)*^{1Amc} (Rodda and McMahon, 2006) and *Efnb2*^{tm1And} mice (Gerety and Anderson, 2002). Except where noted, all controls are littermates, since neonatal mice change their bone structure in a matter of hours. Since perinatal mice grow rapidly, and the *Osx1Cre* transgene has been reported to influence bone structure (Davey et al., 2012; Huang and Olsen, 2015), three parallel breeding colonies were used: (1) *Efnb2*$^{f/f}$ breeders hemizygous for *Osx1Cre*, to provide neonatal *Osx1Cre.Efnb2*$^{\Delta/\Delta}$ and *Efnb2*$^{f/f}$ littermates; (2) wild-type breeders from the same colony that were hemizygous for *Osx1Cre*, to provide neonatal *Osx1Cre.Efnb2*$^{w/w}$ and wild-type littermates; and (3) *Osx1Cre.Efnb2*$^{w/f}$ breeders to generate *Osx1Cre.Efnb2*$^{\Delta/\Delta}$ and *Osx1Cre.Efnb2*$^{w/w}$ littermates for analysis at 6 weeks of age. For chondrocyte cultures, breeding colony 1 was used as the most practical way to provide littermate controls and limit wastage of animals; the lack of *Osx1Cre.Efnb2*$^{w/w}$ littermate cultures might limit the interpretation of those data.

Histology and histomorphometry

Neonatal hind leg and 6-week-old tibia samples were fixed in 4% paraformaldehyde and embedded in methylmethacrylate (Sims et al., 2000) and 5 µm sections were stained with von Kossa, Toluidine Blue, Xylenol Orange or Safranin O/Fast Green as previously described (Poulton et al., 2012). Histomorphometric analysis using OsteoMeasure (OsteoMetrics) was carried out in the proximal tibia, commencing 370 µm from the start of the mineralising zone of the growth plate on Toluidine Blue-stained sections, as previously described (Walker et al., 2008). For analysis of neonatal mice, to correct for slight differences in age that may exist between the litters, all histomorphometric data are presented as a percentage of data obtained from *Osx1Cre*-negative littermate controls. Since *Osx1Cre* mice have been reported to exhibit a neonatal phenotype (Huang and Olsen, 2015), we also examined age-matched wild-type and *Osx1Cre* littermates. Hypertrophic zone width was measured at the centre of the distal femoral growth plates; two sections per mouse were evaluated across 370 µm, avoiding the sides closest to the edge of the bone. No significant alterations in raw BV/TV values were observed between *Efnb2-loxP* mice and age-matched wild-type controls (data not shown). All histomorphometric data include all mice (at least one per genotype per litter) from three litters; n=5-9 per group, including a mixture of male and female neonatal mice.

Micro-computed tomography (microCT)

Ex vivo microCT was performed on femoral specimens using a SkyScan 1076 system (Bruker). Images were acquired with a 0.5 mm aluminium filter at 9 µm pixel size, 50 kV and 100 µA. Houndsfield unit (HU) calibration setting was 125,000 and rotation 0.5°. For neonatal bones, images were reconstructed using NRecon (version 1.6.3.1) with a dynamic image range

Development (2016) 143, 648-657 doi:10.1242/dev.125625

of 0-0.06. DataViewer (version 1.4.4) was used to reorient images, and pseudocoloured images of the whole femur were obtained by volume rendering (CTvox version 2.4.0). The transfer function components (red, green, blue and opacity) were adjusted to the same settings for all samples. CTan (version 1.11.8.0) was used for femoral trabecular analysis; the trabecular region of interest (ROI) was taken as 20% of the total bone length commencing at a site 40% proximal to the distal end. For samples from 6-week-old mice, microCT of the distal femora was performed as previously described (Takyar et al., 2013).

Immunohistochemistry

Hindlimbs from neonatal mice were fixed, decalcified and embedded in paraffin and used for immunohistochemistry as previously described (Sims et al., 1997) with the following modifications. Endogenous peroxidase was inhibited with 0.3% hydrogen peroxide (Merck) in PBS for 30 min, then blocked with 5% normal goat serum in 1% BSA/PBS. Sections were incubated overnight with 1:100 rabbit anti-ADAMTS4 (ab28285, Abcam) in 1% BSA/PBS, followed by 6 µg/ml biotinylated goat anti-rabbit IgG (DakoCytomation) for 1 h and 1.6 mg/ml streptavidin-HRP (DakoCytomation) in PBS for 30 min. ADAMTS4-positive cells were visualised with 0.5 mg/ml diaminobenzidine (Sigma) in PBS, then lightly counterstained with Haematoxylin before dehydration and coverslipping. Four hindlimb sections of each genotype, including both femur and tibia, from two independent litters were assessed. Immunohistochemical staining was carried out on two separate occasions on all sections, and IgG controls were included.

Electron microscopy

Femurs from 1.5- to 2.5-day-old *Efnb2*$^{w/w}$, *Efnb2*$^{f/f}$, *Osx1Cre.Efnb2*$^{\Delta/\Delta}$ and *Osx1Cre.Efnb2*$^{w/w}$ mice (n=3 each) were fixed for a minimum of 24 h in Karnovsky's fixative. Samples were post-fixed in 1% osmium tetroxide/1.5% potassium ferrocyanide for 5 h and embedded in Spurr's resin. Ultrathin sections were stained with uranyl acetate/Reynold's lead citrate and examined with a Philips 300 transmission electron microscope at 60 kV as previously described (Tonna et al., 2014).

Primary chondrocytes

Primary chondrocytes were generated from the rib cages of 2.5- to 4.5-day-old *Osx1Cre.Efnb2*$^{\Delta/\Delta}$ and *Efnb2*$^{f/f}$ littermates using previously described methods (Gosset et al., 2008), with the following modifications. The immature chondrocytes were seeded at a density of 30,000 cells/well into a 3.5 cm plate (Corning) in complete medium (DMEM+10% FBS) and left overnight at 37°C in 5% CO_2. The following day, the plates were placed in 1% O_2, 5% CO_2 and 94% N_2 within a sealed hypoxia chamber (Billups-Rothenberg) at 37°C. Cells were then differentiated for 21 days in chondrocyte differentiation media (Gosset et al., 2008).

Chondrocytic support of osteoclast formation was assessed by co-culture of primary chondrocytes and bone marrow macrophages from C57BL/6 mice (Masuyama et al., 2006) using primary chondrocytes generated as above. To ensure that ephrin B2 had been downregulated, chondrocytes were first differentiated in chondrocyte differentiation media for 21 days at 1% O_2, 5% CO_2 and 94% N_2, as above, then transferred to 37°C under 5% CO_2 for co-culture with bone marrow macrophages.

RNA extraction and RT-PCR

Total RNA was extracted from primary chondrocytes and quantitative RT-PCR was performed using previously described methods (Tonna et al., 2014). Primers are listed in Table S1. Data shown in Fig. 5B were calculated by normalising to the geometric mean of the two housekeeping genes *Hprt1* and *B2m* using the ΔCt method, and fold-change calculations using the ΔΔCt method were performed as previously described (Chia et al., 2015).

Statistical methods

All statistical tests were carried out using Prism 6. Data shown in Fig. 1B, Fig. 3B and Fig. 5B were analysed by two-way ANOVA. Data shown in Fig. 2C, Fig. 5A and Table 2 were analysed by Student's t-test. P<0.05 was considered significant.

Competing interests

The authors declare no competing or financial interests.

Author contributions

S.T., I.J.P., F.T., B.C.-I., N.E.M., B.T., P.W.M.H., L.T. and N.A.S. conducted experiments and analysed data. S.T., N.A.S., L.T., E.J.M. and T.J.M. designed experiments and interpreted data. The manuscript was prepared by S.T. and N.A.S., and edited by S.T., N.A.S., E.J.M. and T.J.M. All authors read and approved the final manuscript.

Funding

This work was supported by National Health and Medical Research Council (Australia) (NHMRC) Project Grants [620200 and 104129]. N.A.S. is supported by an NHMRC Senior Research Fellowship. S.T. received support from an NHMRC Peter Doherty Early Career Fellowship. The Victorian State Government Operational Infrastructure Support Scheme provides support to St Vincent's Institute.

Supplementary information

Supplementary information available online at
http://dev.biologists.org/lookup/suppl/doi:10.1242/dev.125625/-/DC1

References

Allan, E. H., Hausler, K. D., Wei, T., Gooi, J. H., Quinn, J. M. W., Crimeen-Irwin, B., Pompolo, S., Sims, N. A., Gillespie, M. T., Onyia, J. E. et al. (2008). EphrinB2 regulation by PTH and PTHrP revealed by molecular profiling in differentiating osteoblasts. *J. Bone Miner. Res.* **23**, 1170-1181.

Blair, H. C., Yaroslavskiy, B. B., Robinson, L. J., Mapara, M. Y., Pangrazio, A., Guo, L., Chen, K., Vezzoni, P., Tolar, J. and Orchard, P. J. (2009). Osteopetrosis with micro-lacunar resorption because of defective integrin organization. *Lab. Invest.* **89**, 1007-1017.

Bond, S. R., Lau, A., Penuela, S., Sampaio, A. V., Underhill, T. M., Laird, D. W. and Naus, C. C. (2011). Pannexin 3 is a novel target for Runx2, expressed by osteoblasts and mature growth plate chondrocytes. *J. Bone Miner. Res.* **26**, 2911-2922.

Buenzli, P. R. and Sims, N. A. (2015). Quantifying the osteocyte network in the human skeleton. *Bone* **75**, 144-150.

Chambers, T. J. and Fuller, K. (1985). Bone cells predispose bone surfaces to resorption by exposure of mineral to osteoclastic contact. *J. Cell Sci.* **76**, 155-165.

Chambers, T. J., Darby, J. A. and Fuller, K. (1985). Mammalian collagenase predisposes bone surfaces to osteoclastic resorption. *Cell Tissue Res.* **241**, 671-675.

Chen, J., Shi, Y., Regan, J., Karuppaiah, K., Ornitz, D. M. and Long, F. (2014). Osx-Cre targets multiple cell types besides osteoblast lineage in postnatal mice. *PLoS ONE* **9**, e85161.

Chia, L. Y., Walsh, N. C., Martin, T. J. and Sims, N. A. (2015). Isolation and gene expression of haematopoietic-cell-free preparations of highly purified murine osteocytes. *Bone* **72**, 34-42.

Chiusaroli, R., Maier, A., Knight, M. C., Byrne, M., Calvi, L. M., Baron, R., Krane, S. M. and Schipani, E. (2003). Collagenase cleavage of type I collagen is essential for both basal and parathyroid hormone (PTH)/PTH-related peptide receptor-induced osteoclast activation and has differential effects on discrete bone compartments. *Endocrinology* **144**, 4106-4116.

Cielinski, M. J. and Marks, S. C., Jr. (1994). Neonatal reductions in osteoclast number and function account for the transient nature of osteopetrosis in the rat mutation microphthalmia blanc (mib). *Bone* **15**, 707-715.

Cielinski, M. J. and Marks, S. C., Jr. (1995). Bone metabolism in the osteopetrotic rat mutation microphthalmia blanc. *Bone* **16**, 567-574.

Davey, R. A., Clarke, M. V., Sastra, S., Skinner, J. P., Chiang, C., Anderson, P. H. and Zajac, J. D. (2012). Decreased body weight in young Osterix-Cre transgenic mice results in delayed cortical bone expansion and accrual. *Transgenic Res.* **21**, 885-893.

Del Fattore, A., Cappariello, A. and Teti, A. (2008). Genetics, pathogenesis and complications of osteopetrosis. *Bone* **42**, 19-29.

Gao, S.-G., Zeng, C., Song, Y., Tian, J., Cheng, C., Yang, T., Li, H., Zhang, F.-J. and Lei, G.-H. (2015). Effect of osteopontin on the mRNA expression of ADAMTS4 and ADAMTS5 in chondrocytes from patients with knee osteoarthritis. *Exp. Ther. Med.* **9**, 1979-1983.

Gerety, S. S. and Anderson, D. J. (2002). Cardiovascular ephrinB2 function is essential for embryonic angiogenesis. *Development* **129**, 1397-1410.

Gil-Henn, H., Destaing, O., Sims, N. A., Aoki, K., Alles, N., Neff, L., Sanjay, A., Bruzzaniti, A., De Camilli, P., Baron, R. et al. (2007). Defective microtubule-dependent podosome organization in osteoclasts leads to increased bone density in Pyk2(–/–) mice. *J. Cell Biol.* **178**, 1053-1064.

Glasson, S. S., Askew, R., Sheppard, B., Carito, B. A., Blanchet, T., Ma, H.-L., Flannery, C. R., Kanki, K., Wang, E., Peluso, D. et al. (2004). Characterization of and osteoarthritis susceptibility in ADAMTS-4-knockout mice. *Arthritis Rheum.* **50**, 2547-2558.

Golovchenko, S., Hattori, T., Hartmann, C., Gebhardt, M., Gebhard, S., Hess, A., Pausch, F., Schlund, B. and von der Mark, K. (2013). Deletion of beta catenin in hypertrophic growth plate chondrocytes impairs trabecular bone formation. *Bone* **55**, 102-112.

Gosset, M., Berenbaum, F., Thirion, S. and Jacques, C. (2008). Primary culture and phenotyping of murine chondrocytes. *Nat. Protoc.* **3**, 1253-1260.

Hayman, A. R., Jones, S. J., Boyde, A., Foster, D., Colledge, W. H., Carlton, M. B., Evans, M. J. and Cox, T. M. (1996). Mice lacking tartrate-resistant acid phosphatase (Acp 5) have disrupted endochondral ossification and mild osteopetrosis. *Development* **122**, 3151-3162.

Holliday, L. S., Welgus, H. G., Fliszar, C. J., Veith, G. M., Jeffrey, J. J. and Gluck, S. L. (1997). Initiation of osteoclast bone resorption by interstitial collagenase. *J. Biol. Chem.* **272**, 22053-22058.

Huang, W. and Olsen, B. (2015). Skeletal defects in Osterix-Cre transgenic mice. *Transgenic Res.* **24**, 167-172.

Ito, M., Tokunaga, K., Kitahara, H., Ito, T., Kondoh, N. and Endo, N. (2006). ephrinB2 and EphB4 are expressed on the chondrocyte during fracture healing. *Acta Med. Biol.* **54**, 21-31.

Iwamoto, T., Nakamura, T., Doyle, A., Ishikawa, M., de Vega, S., Fukumoto, S. and Yamada, Y. (2010). Pannexin 3 regulates intracellular ATP/cAMP levels and promotes chondrocyte differentiation. *J. Biol. Chem.* **285**, 18948-18958.

Johansson, N., Saarialho-Kere, U., Airola, K., Herva, R., Nissinen, L., Westermarck, J., Vuorio, E., Heino, J. and Kähäri, V.-M. (1997). Collagenase-3 (MMP-13) is expressed by hypertrophic chondrocytes, periosteal cells, and osteoblasts during human fetal bone development. *Dev. Dyn.* **208**, 387-397.

Kartsogiannis, V., Zhou, H., Horwood, N. J., Thomas, R. J., Hards, D. K., Quinn, J. M., Niforas, P., Ng, K. W., Martin, T. J. and Gillespie, M. T. (1999). Localization of RANKL (receptor activator of NF kappa B ligand) mRNA and protein in skeletal and extraskeletal tissues. *Bone* **25**, 525-534.

Kosaki, N., Takaishi, H., Kamekura, S., Kimura, T., Okada, Y., Minqi, L., Amizuka, N., Chung, U.-I., Nakamura, K., Kawaguchi, H. et al. (2007). Impaired bone fracture healing in matrix metalloproteinase-13 deficient mice. *Biochem. Biophys. Res. Commun.* **354**, 846-851.

Li, Y.-P., Chen, W., Liang, Y., Li, E. and Stashenko, P. (1999). Atp6i-deficient mice exhibit severe osteopetrosis due to loss of osteoclast-mediated extracellular acidification. *Nat. Genet.* **23**, 447-451.

Lian, J. B., McKee, M. D., Todd, A. M. and Gerstenfeld, L. C. (1993). Induction of bone-related proteins, osteocalcin and osteopontin, and their matrix ultrastructural localization with development of chondrocyte hypertrophy in vitro. *J. Cell. Biochem.* **52**, 206-219.

Maes, C., Kobayashi, T., Selig, M. K., Torrekens, S., Roth, S. I., Mackem, S., Carmeliet, G. and Kronenberg, H. M. (2010). Osteoblast precursors, but not mature osteoblasts, move into developing and fractured bones along with invading blood vessels. *Dev. Cell* **19**, 329-344.

Marks, S. C. (1973). Pathogenesis of osteopetrosis in the ia rat: reduced bone resorption due to reduced osteoclast function. *Am. J. Anat.* **138**, 165-189.

Masuyama, R., Stockmans, I., Torrekens, S., Van Looveren, R., Maes, C., Carmeliet, P., Bouillon, R. and Carmeliet, G. (2006). Vitamin D receptor in chondrocytes promotes osteoclastogenesis and regulates FGF23 production in osteoblasts. *J. Clin. Invest.* **116**, 3150-3159.

Monaghan, B. A., Kaplan, F. S., August, C. S., Fallon, M. D. and Flannery, D. B. (1991). Transient infantile osteopetrosis. *J. Pediatr.* **118**, 252-256.

Nakamura, M., Sone, S., Takahashi, I., Mizoguchi, I., Echigo, S. and Sasano, Y. (2005). Expression of versican and ADAMTS1, 4, and 5 during bone development in the rat mandible and hind limb. *J. Histochem. Cytochem.* **53**, 1553-1562.

Neutzsky-Wulff, A. V., Sims, N. A., Supanchart, C., Kornak, U., Felsenberg, D., Poulton, I. J., Martin, T. J., Karsdal, M. A. and Henriksen, K. (2010). Severe developmental bone phenotype in ClC-7 deficient mice. *Dev. Biol.* **344**, 1001-1010.

Othman-Hassan, K., Patel, K., Papoutsi, M., Rodriguez-Niedenfuhr, M., Christ, B. and Wilting, J. (2001). Arterial identity of endothelial cells is controlled by local cues. *Dev. Biol.* **237**, 398-409.

Park, J., Gebhardt, M., Golovchenko, S., Perez-Branguli, F., Hattori, T., Hartmann, C., Zhou, X., deCrombrugghe, B., Stock, M., Schneider, H. et al. (2015). Dual pathways to endochondral osteoblasts: a novel chondrocyte-derived osteoprogenitor cell identified in hypertrophic cartilage. *Biol. Open* **4**, 608-621.

Pasquale, E. B. (2010). Eph receptors and ephrins in cancer: bidirectional signalling and beyond. *Nat. Rev. Cancer* **10**, 165-180.

Poulton, I. J., McGregor, N. E., Pompolo, S., Walker, E. C. and Sims, N. A. (2012). Contrasting roles of leukemia inhibitory factor in murine bone development and remodeling involve region-specific changes in vascularization. *J. Bone Miner. Res.* **27**, 586-595.

Rodda, S. J. and McMahon, A. P. (2006). Distinct roles for Hedgehog and canonical Wnt signaling in specification, differentiation and maintenance of osteoblast progenitors. *Development* **133**, 3231-3244.

Rogerson, F. M., Stanton, H., East, C. J., Golub, S. B., Tutolo, L., Farmer, P. J. and Fosang, A. J. (2008). Evidence of a novel aggrecan-degrading activity in cartilage: studies of mice deficient in both ADAMTS-4 and ADAMTS-5. *Arthritis Rheum.* **58**, 1664-1673.

Schwab, W., Hofer, A. and Kasper, M. (1998). Immunohistochemical distribution of connexin 43 in the cartilage of rats and mice. *Histochem. J.* **30**, 413-419.

Shinoda, Y., Ogata, N., Higashikawa, A., Manabe, I., Shindo, T., Yamada, T., Kugimiya, F., Ikeda, T., Kawamura, N., Kawasaki, Y. et al. (2008). Kruppel-like factor 5 causes cartilage degradation through transactivation of matrix metalloproteinase 9. *J. Biol. Chem.* **283**, 24682-24689.

Sims, N. A., White, C. P., Sunn, K. L., Thomas, G. P., Drummond, M. L., Morrison, N. A., Eisman, J. A. and Gardiner, E. M. (1997). Human and murine osteocalcin gene expression: conserved tissue restricted expression and divergent responses to 1,25-dihydroxyvitamin D3 in vivo. *Mol. Endocrinol.* **11**, 1695-1708.

Sims, N. A., Clement-Lacroix, P., Da Ponte, F., Bouali, Y., Binart, N., Moriggl, R., Goffin, V., Coschigano, K., Gaillard-Kelly, M., Kopchick, J. et al. (2000). Bone homeostasis in growth hormone receptor-null mice is restored by IGF-I but independent of Stat5. *J. Clin. Invest.* **106**, 1095-1103.

Soriano, P., Montgomery, C., Geske, R. and Bradley, A. (1991). Targeted disruption of the c-src proto-oncogene leads to osteopetrosis in mice. *Cell* **64**, 693-702.

Takyar, F. M., Tonna, S., Ho, P. W. M., Crimeen-Irwin, B., Baker, E. K., Martin, T. J. and Sims, N. A. (2013). EphrinB2/EphB4 inhibition in the osteoblast lineage modifies the anabolic response to parathyroid hormone. *J. Bone Miner. Res.* **28**, 912-925.

Tonna, S. and Sims, N. A. (2014). Talking among ourselves: paracrine control of bone formation within the osteoblast lineage. *Calcif. Tissue Int.* **94**, 35-45.

Tonna, S., Takyar, F. M., Vrahnas, C., Crimeen-Irwin, B., Ho, P. W. M., Poulton, I. J., Brennan, H. J., McGregor, N. E., Allan, E. H., Nguyen, H. et al. (2014). EphrinB2 signaling in osteoblasts promotes bone mineralization by preventing apoptosis. *FASEB J.* **28**, 4482-4496.

Touaitahuata, H., Cres, G., de Rossi, S., Vives, V. and Blangy, A. (2014). The mineral dissolution function of osteoclasts is dispensable for hypertrophic cartilage degradation during long bone development and growth. *Dev. Biol.* **393**, 57-70.

Walker, E. C., McGregor, N. E., Poulton, I. J., Pompolo, S., Allan, E. H., Quinn, J. M. W., Gillespie, M. T., Martin, T. J. and Sims, N. A. (2008). Cardiotrophin-1 is an osteoclast-derived stimulus of bone formation required for normal bone remodeling. *J. Bone Miner. Res.* **23**, 2025-2032.

Wang, K., Vishwanath, P., Eichler, G. S., Al-Sebaei, M. O., Edgar, C. M., Einhorn, T. A., Smith, T. F. and Gerstenfeld, L. C. (2006). Analysis of fracture healing by large-scale transcriptional profile identified temporal relationships between metalloproteinase and ADAMTS mRNA expression. *Matrix Biol.* **25**, 271-281.

Wang, Y., Menendez, A., Fong, C., ElAlieh, H. Z., Chang, W. and Bikle, D. D. (2014). Ephrin B2/EphB4 mediates the actions of IGF-I signaling in regulating endochondral bone formation. *J. Bone Miner. Res.* **29**, 1900-1913.

Yang, G., Zhu, L., Hou, N., Lan, Y., Wu, X.-M., Zhou, B., Teng, Y. and Yang, X. (2014a). Osteogenic fate of hypertrophic chondrocytes. *Cell Res.* **24**, 1266-1269.

Yang, L., Tsang, K. Y., Tang, H. C., Chan, D. and Cheah, K. S. E. (2014b). Hypertrophic chondrocytes can become osteoblasts and osteocytes in endochondral bone formation. *Proc. Natl. Acad. Sci. USA* **111**, 12097-12102.

Zhao, C., Irie, N., Takada, Y., Shimoda, K., Miyamoto, T., Nishiwaki, T., Suda, T. and Matsuo, K. (2006). Bidirectional ephrinB2-EphB4 signaling controls bone homeostasis. *Cell Metab.* **4**, 111-121.

Zhou, X., von der Mark, K., Henry, S., Norton, W., Adams, H. and de Crombrugghe, B. (2014). Chondrocytes transdifferentiate into osteoblasts in endochondral bone during development, postnatal growth and fracture healing in mice. *PLoS Genet.* **10**, e1004820.

Table S1. Primers used for RT-PCR

Gene	Primer sequence	GenBank accession no and reference, if published
Adamts4	F 5′-GGAACGGTGGCAAGTATTG-3′ R 5′-CAGGTGAGTTTGCATTGGTC-3′	NM_172845.2
Adamts5	F 5′-GGCATCATTCATGTGACACC-3′ R 5′-CGAGTACTCAGGCCCAAATG-3′	NM_011782.2 (Stanton et al., 2005)
B2m	F 5′-TTCACCCCCACTGAGACTGAT-3′ R 5′-GTCTTGGGCTCGGCCATA-3′	NM_013556 (Purton et al., 2006)
Col10a1	F 5′-TGGTTCATGGGATGTTTTATGC-3′ R 5′-GGCTAGCAAGTGGGCCCT-3′	NM_009925.4
Efnb2	F 5′-AGAACTGGGAGCGGCTTG-3′ R 5′-TGGCCAACAGTTTTAGAGTCG-3′	NM_010111.5 (Tonna et al., 2014)
Hprt1	F 5′-TGATTAGCGATGATGAACCAG-3′ R 5′-AGAGGGCCACAATGTGATG-3′	NM_013556 (Kartsogiannis et al., 2008)
Mmp3	F 5′-TCCCTCTATGGAACTCCCACAGC-3′ R 5′-TTCTCCCCGGAGGGTGCTGAC-3′	NM_010809.1 (Le Goff et al., 2014)
Mmp9	F 5′-GAGTCCGGCAGACAATCCTT-3′ R 5′-CTTCCAGTACCAACCGTCCT-3′	NM_013599.3
Mmp13	F 5′-TGGGCTCTGAATGGTTATGA-3′ R 5′-AACTCCACACGTGGTTCTCA-3′	NM_008607.2
Sp7	F 5′-TATGCTCCGACCTCCTCAAC-3′ R 5′-AATAAGATTGGGAAGCAGAAAG-3′	NM_130458.3 (Allan et al., 2008)
Spp1	F 5′-TAGCTTGGCTTATGGACTGAGG-3′ R 5′-AGACTCACCGCTCTTCATGTG-3′	NM_001204201.1 (Nakamura et al., 2007)
Tnfsf11	F 5′-AACATTTGCTTTCGGCATC-3′ R 5′-TTTCGTGCTCCCTCCTTTC-3′	NM_011613.3 (Allan et al., 2008)
Tnfrsf11b	F 5′-CCTACCTAAAACAGCACTGCAC-3′ R 5′-TAACGCCCTTCCTCACACTC-3′	NM_008764.3 (Stanton et al., 2005; Allan et al., 2008)

Supplementary references

Kartsogiannis, V., Sims, N. A., Quinn, J. M. W., Ly, C., Cipetic, M., Poulton, I. J., Walker, E. C., Saleh, H., McGregor, N. E., Wallace, M. E. et al. (2008). Osteoclast inhibitory lectin, an immune cell product that is required for normal bone physiology in vivo. *J. Biol. Chem.* **283**, 30850-30860.

Le Goff, B., Singbrant, S., Tonkin, B. A., Martin, T. J., Romas, E., Sims, N. A. and Walsh, N. C. (2014). Oncostatin M acting via OSMR, augments the actions of IL-1 and TNF in synovial fibroblasts. *Cytokine* **68**, 101-109.

Nakamura, A., Ly, C., Cipetic, M., Sims, N. A., Vieusseux, J., Kartsogiannis, V., Bouralexis, S., Saleh, H., Zhou, H., Price, J. T. et al. (2007). Osteoclast inhibitory lectin (OCIL) inhibits osteoblast differentiation and function in vitro. *Bone* **40**, 305-315.

Purton, L. E., Dworkin, S., Olsen, G. H., Walkley, C. R., Fabb, S. A., Collins, S. J. and Chambon, P. (2006). RARgamma is critical for maintaining a balance between hematopoietic stem cell self-renewal and differentiation. *J. Exp. Med.* **203**, 1283-1293.

Stanton, H., Rogerson, F. M., East, C. J., Golub, S. B., Lawlor, K. E., Meeker, C. T., Little, C. B., Last, K., Farmer, P. J., Campbell, I. K. et al. (2005). ADAMTS5 is the major aggrecanase in mouse cartilage in vivo and in vitro. *Nature* **434**, 648-652.